

Article

# Synchronous Power Control of Grid-Connected Power Converters under Asymmetrical Grid Fault

Weiyi Zhang <sup>1,\*</sup> , Joan Rocabert <sup>1</sup>, J. Ignacio Candela <sup>1</sup>  and Pedro Rodriguez <sup>1,2</sup>

<sup>1</sup> Electrical Engineering Department, Technical University of Catalonia, Barcelona 08222, Spain; rocabert@ee.upc.edu (J.R.); candela@ee.upc.edu (J.I.C.); prodriguez@uloyola.es (P.R.)

<sup>2</sup> Department of Engineering, Loyola University of Andalucia, Seville 41014, Spain

\* Correspondence: weiyi.zhang@estudiant.upc.edu; Tel.: +34-93-739-8291

Academic Editor: Jayanta Deb Mondol

Received: 6 June 2017; Accepted: 5 July 2017; Published: 8 July 2017

**Abstract:** Control of grid-connected power converters is continuously developing to meet the grid codes, according to which the generation units should keep connected to the grid and further provide ancillary services, such as voltage and frequency support, negative sequence current injection, inertia emulation, etc. A virtual admittance controller is proposed in this paper for the objective of voltage support under asymmetrical grid faults. By using independent and selective admittances for positive and negative sequence current injection, the unbalanced voltage can be significantly compensated during asymmetrical faults. The controller is based on the generic control framework of the synchronous power controller (SPC), which is able to control a power converter with emulated and improved synchronous generator characteristics. Simulation and experimental results based on two paralleled 100 kW grid-connected power converters demonstrate the controller to be effective in supporting unbalanced voltage sags.

**Keywords:** sodium-ion battery; cathode; grid-connected power converter; power converter control; synchronous power controller; virtual admittance

## 1. Introduction

Grid-connected power converters have been acting as an important interface between the renewables and the electrical grids. The conventional control of grid-connected power converters has been well validated in many applications and shows its effectiveness [1–4]. Along with the expansion of the renewable power generation plants, their impact on the power system has caused increasing attention [5,6]. The different performance of the converters compared to the traditional synchronous generators should be taken into account.

The conventional grid-connected power converters differ from synchronous generators mainly in the lack of the electromechanical characteristics. Consequently, the statics and dynamics of the renewable power generation units are both different compared with the synchronous generators. Even if the statics can be changed by equipping the droop control and energy reserve, there are still some disadvantages of the converter-interfaced generation plants.

The phase-locked loop (PLL) is a grid voltage estimator used by conventional power converters to obtain the voltage phase angle to determine the amount of current to be injected either in-phase or in-quadrature to regulate the active and reactive powers delivered to the grid, respectively. Therefore, the dynamics of these conventional converters are characterized by the PLL, whose performance will degrade under weak or islanded grid conditions [7,8]. As a PLL is not designed to emulate any inertial response in the presence of frequency deviations, the total inertia in the grid decreases as the integration of renewable generation plants grows. However, the updated grid codes have included “synthetic inertia” in the grid connection requirements [9].

The emulation of synchronous generators and the implementation of its mechanical and electrical characteristics on grid-connected converters have been intensively studied in recent years. The implementation of mechanical characteristics, especially rotor inertia emulation, has been investigated in many studies to contribute with synthetic inertia to the power system [10–12]. Besides, the emulation of electrical characteristics, commonly known as virtual impedance, is also largely developed for objectives such as the load sharing of paralleled converters [13,14], harmonics compensation [15,16] and impedance shaping in cascaded converters [17]. Nevertheless, the performance of the synchronous generation emulation control under grid faults, especially under asymmetrical faults, still needs further study.

Grid-connected power converters can face voltage sags caused by different types of grid faults. According to grid code requirements, grid-connected power converters should be capable of getting through grid fault scenarios to let generation units remain connected under such adverse conditions, and further provide ancillary services to support the grid voltage and frequency.

Three-phase balanced faults are usually considered for stating the low-voltage ride-through (LVRT) requirements in most of the grid codes; however, asymmetrical faults are the most common faults in electrical grids [18,19]. Due to an asymmetrical grid fault, the voltages at the point of common coupling (PCC) will sag and become unbalanced, and may cause the trip of the power converters and the loads connected to the PCC. Sophisticated ride-through abilities for power converters can be enabled to prevent tripping of renewable generation units under fault conditions [20,21], the lack of contribution of negative-sequence current during asymmetrical faults motivates further improvement in the control design [22].

Many previous works have proposed techniques to deal with the grid synchronization of power converters during asymmetrical grid faults. Smith et al. [23] has presented different variations of synchronous reference frame PLL for grid synchronization, which are able to decompose the positive and negative components of grid voltage, even under unbalanced conditions. Alternative methods such as [24] using a Kalman filter have also been presented for the power converters to be synchronized to the grid under both balanced and unbalanced voltage sags. As is known, unbalanced voltages contain both positive-sequence component and negative-sequence component. In order to compensate the negative-sequence component of the PCC voltages, the current injected by the power converter should also contain a negative-sequence component, as well as the positive-sequence one. Therefore, the injection of negative-sequence current by a generation unit should be also considered as an objective, in addition to grid synchronization.

This paper develops a virtual admittance control structure, which is a part of the synchronous power controller (SPC) for grid-connected power converters. The SPC is an established solution for controlling grid-connected power converters and equipping them with emulated and improved synchronous machine characteristics. In the proposed virtual admittance block, except for the emulation of the stator output impedance of the synchronous generators, extra function of injecting negative-sequence current under asymmetrical grid faults is also added. Simulation and experimental results based on two parallel connected 100 kW grid-connected power converters are presented in this paper to demonstrate the effectiveness of the proposed control strategy in realizing negative-sequence current injection, as well as the basic function of the virtual admittance.

Unlike previous works that emphasize the grid synchronization of power converters under unbalanced grid voltages, this work implements a different control framework, the SPC, for grid-connected power converters to contribute emulated and improved synchronous generator characteristics to the grid. Furthermore, it is also shown that its capability of injecting negative-sequence reactive current during asymmetrical grid fault using a specially designed tri-path virtual admittance block.

The rest of the paper is organized as follows. The general control framework of the SPC with the proposed virtual admittance control structure are elaborated in Section 2. Section 3 shows the detailed design of the virtual admittance block considering the E.ON and Red Electrica

de Espana (REE) grid codes. The simulation results under asymmetrical faults are shown in Section 4. The experimental results under the same fault condition are shown in Section 5.

## 2. Synchronous Power Controller with Selective Virtual Admittances

The main synchronous generator characteristics contain two aspects, the stator output impedance (electrical) and the rotor inertia (mechanical). The former one defines the fundamentals of active and reactive power generation, which is important in grid synchronization, load sharing, etc. The latter one affects the dynamics of the power system and ensures the instantaneous power balance. The SPC aims to equip grid-connected power converters with aforementioned characteristics, while this paper mainly addresses its virtual admittance block design with special function of negative-sequence current control.

### 2.1. Synchronous Power Controller

Figure 1 shows the cascaded control layers of the SPC-based grid-connected converters. The SPC mainly consists of the electrical part and the mechanical part, corresponding to the electrical and mechanical part of the synchronous generators.

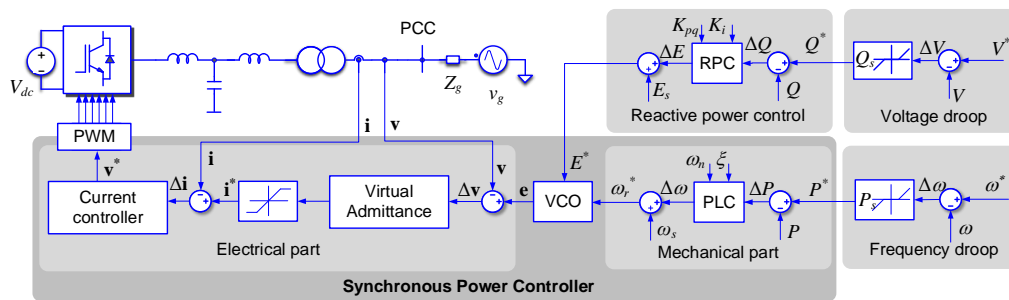


Figure 1. Control of grid-connected power converters based on the synchronous power controller (SPC).

The mechanical part of the SPC generates the reference frequency,  $\omega_r^*$ , which corresponds to the inner frequency of a synchronous generator, and it swings around the rated frequency  $\omega_s$  following the relation expressed as:

$$\omega_r^* = \omega_s + (P^* - P) \frac{\omega_n^2 / P_{max}}{s + 2\zeta\omega_n} \quad (1)$$

where  $P^*$  is the active power reference,  $P$  the generated active power,  $P_{max}$  is a transmission gain between the load angle and the generated power used in the active power control loop modeling,  $\zeta$ , and,  $\omega_n$ , the damping factor and the natural frequency of the second-order power loop transfer function.

Since the form of Equation (1) is deduced based on the dynamics of the generator rotor,  $\omega_n$  can be translated to the inertia constant,  $H$ , following Equation (2). In this way, the virtual mechanical characteristic can be set:

$$\omega_n = \sqrt{\frac{P_{max}\omega_s}{2HS_n}} \quad (2)$$

where  $S_n$  the rated power of the converter.

The voltage controlled oscillator (VCO) block generates the virtual electromotive force,  $e$ , using  $\omega_r^*$  and the magnitude reference,  $E^*$ , which is generated by the reactive power controller. In the case when the electrical part control is realized in the stationary reference frame, the VCO can be expressed as:

$$\mathbf{e} = \begin{bmatrix} e_\alpha \\ e_\beta \end{bmatrix} = \begin{bmatrix} E^* \cos(\omega_r^* t) \\ E^* \sin(\omega_r^* t) \end{bmatrix} \quad (3)$$

where the phase of  $\mathbf{e}$  is obtained by integrating  $\omega_r^*$ , similar to the function of the VCO in a PLL.

The electrical part includes the virtual admittance and the current controller. The current controller let the converter inject the current following the reference that is defined by the virtual admittance block. In the case when the control is implemented in the stationary reference frame, the Proportional Resonant controller is used and expressed as

$$\mathbf{v}_{\alpha\beta}^* = (\mathbf{i}_{\alpha\beta}^* - \mathbf{i}_{\alpha\beta})(K_p + K_r \frac{k_{bw}\omega s}{s^2 + k_{bw}\omega s + \omega^2}) \tag{4}$$

As shown in Figure 1, the reactive power controller (RPC) and the outer  $P$ - $f$  and  $Q$ - $V$  droop loops are also needed as complementary part of the SPC. A proportional integral (PI) controller is usually used as the RPC and expressed as:

$$E^* = E_s + (Q^* - Q)(K_{pq} + \frac{K_i}{s}) \tag{5}$$

The outer droop controllers are expressed as:

$$P^* = P_s + (\omega^* - \omega)D_p \tag{6}$$

$$Q^* = Q_s + (V^* - V)D_q \tag{7}$$

### 2.2. Proposed Virtual Admittance Block

The SPC's virtual admittance block, as Figure 1 shows, defines an output admittance for the power converter equivalent to the output impedance of a synchronous generator. The admittance structure used in the admittance block can be written as:

$$i^* = \frac{e - v}{R + sL} \tag{8}$$

As an enhancement to the output impedance of a synchronous generator, multiple and selective admittances are proposed to be built up in this block, as shown in Figure 2. Different impedance values for the positive- and negative-sequence signals can be used to achieve different levels of positive- and negative-sequence current injection during the voltage sags.

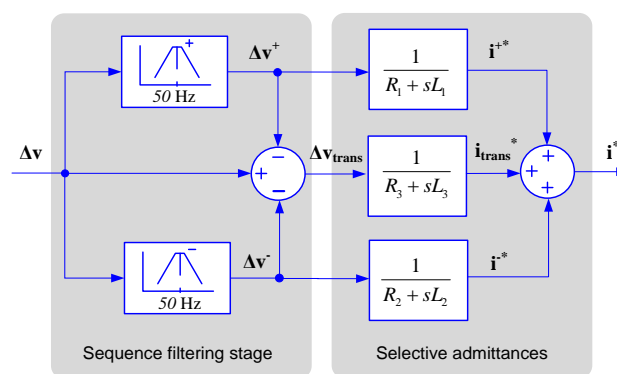


Figure 2. Virtual admittance block for positive- and negative-sequence current injection.

In Figure 2,  $L_1$  and  $R_1$  are the inductance and the damping resistance of the impedance for the positive-sequence voltage components at the fundamental frequency, while  $L_2$  and  $R_2$  are the ones for the negative-sequence signals at the fundamental frequency. The rest of the voltage components go through a third admittance branch ( $L_3$  and  $R_3$ ), which is named as transient admittance. Considering the possible delay of the filtering stages, this third branch will present a controlled impedance feature

during transients. Therefore, the positive- and negative-sequence voltage support possess the same gain during the transient, which is determined by  $L_3$ . In addition, the injection of harmonic currents is also determined by this transient admittance, although additional selective band-pass filters and corresponding harmonic impedances might be also implemented. Above all, the current reference generated by the virtual admittance block of Figure 2 results from the sum of three components, that is:

$$\mathbf{i}^* = \mathbf{i}^{+*} + \mathbf{i}^{-*} + \mathbf{i}_{trans}^* \quad (9)$$

The proposed virtual admittance has several advantages compared with the physical stator impedance of synchronous generators. Firstly, the positive- and negative-sequence voltages are decomposed and processed through difference admittances. Further, the delay effect of the positive- and negative-sequence components calculation is considered and hence a third general admittance branch is included as a compensation. Moreover, the admittance values of each branch can be online adjusted to meet the requirements in the full operation stage. In detail, the admittance values can be specified much smaller than the nominal ones during grid connection operations to avoid large transient currents caused by the transient lack of synchronization between the grid voltage and the converter inner-built electromotive force. Then the admittance values can be conditioned to the nominal ones within a specified time of transition.

For separating the positive- and negative-sequence signals, sequence band-pass filters are needed in a former stage. The design of this sequence band-pass filters for this objective has been addressed in many works, such as [25]. In this paper the method used is based on the dual second-order generalized integrator (D-SOGI), which can be expressed as:

$$\mathbf{v}_{\alpha\beta}^+ = \frac{1}{2} \begin{bmatrix} f_d & -f_q \\ f_q & f_d \end{bmatrix} \mathbf{v}_{\alpha\beta} \quad (10a)$$

$$\mathbf{v}_{\alpha\beta}^- = \frac{1}{2} \begin{bmatrix} f_d & f_q \\ -f_q & f_d \end{bmatrix} \mathbf{v}_{\alpha\beta} \quad (110b)$$

where the resonant and quadrature output of the SOGI, namely,  $f_d(s)\mathbf{v}_{\alpha\beta}$  and  $f_q(s)\mathbf{v}_{\alpha\beta}$ , are used to generate the positive- and negative-sequence signals.  $f_d(s)$  and  $f_q(s)$  in Equation (10) have the transfer functions as:

$$f_d(s) = \frac{k_{bw}\omega s}{s^2 + k_{bw}\omega s + \omega^2} \quad (11a)$$

$$f_q(s) = \frac{k_{bw}\omega^2}{s^2 + k_{bw}\omega s + \omega^2} \quad (11b)$$

where  $k_{bw}$  is the bandwidth parameter and  $\omega$  is the center frequency.

### 2.3. Design Considerations

The virtual admittance block has to be carefully designed to achieve the desired performance in both normal operation and voltage sag conditions. Moreover, in addition to meet requirements regarding magnitude of the current injection to be injected during the voltage sags, the time response should also be considered.

#### 2.3.1. Grid Code Requirements

Different requirements of reactive current injection during voltage dips can be found in grid codes. The proportional gain between the reactive current to be injected,  $I_q$ , and the voltage drop magnitude,  $\Delta V$ , can be defined to set the minimum requirement for the voltage support, which is written as:

$$I_q^{pu} \geq -k_q \Delta V_{pu} \quad (12)$$

In this paper, a convention of the sign of the reactive current is defined to let the reactive power have a positive value under leading operation, and hence a negative value under lagging operation. In this way, as shown in Equation (12), the injected reactive current has a positive value when the grid voltage drops.

In the E.ON grid codes, a proportional gain for reactive current injection,  $k_q$ , is required to be equal to or greater than 2, and the operational region for voltage regulation has a higher bound of  $1.2 V_N$ , being  $V_N$  the rated grid voltage, which provides voltage limitation as well as voltage support, and a dead band of  $\pm 5\%$  around  $V_N$  [26].

In the REE (the Spanish electrical grid operator) grid codes, it is required that the voltage support by reactive current injection should be activated once the voltage is lower than 85% of its rated value, and the reactive current should reach 90% when the voltage is lower than 50% of its rated value [27]. Based on these critical points, the proportional gain for reactive current injection,  $k_q$ , is calculated to be equal to or greater than 2.57.

Regarding the cases of asymmetrical faults, according to the European Network of Transmission System Operators for Electricity (ENTSO-E) grid codes, the fault-ride-through capabilities should be defined by each transmission system operator (TSO), while respecting the provisions of the national regulatory authorities [9].

One example of the requirement of the negative-sequence current injection can be found in the German grid codes VDE-AR-N 4120 [28], where it is required a proportional gain  $k_2$  between the magnitude of the negative-sequence current and the negative-sequence voltage given by:

$$I^- = k_2(\Delta V^- - 0.05) \quad (13)$$

where  $k_2$  represent the regulation gain, required to be within the range of 0 to 10, and  $\Delta V^-$  is the incremental change of the magnitude of the negative-sequence voltage. As a complement of this relationship, there is a saturation for the magnitude of the negative-sequence current  $I^-$  at 1 p.u..

Moreover, the following specifications can be found in the grid codes regarding requirements of the time response of the voltage support.

In the E.ON grid codes, it is stated that the voltage support service of the generation unit needs to be activated when a voltage dip of over 5% of the rms value of the generator voltage occurs, and the voltage support should occur within 20 ms after fault detection.

In the REE grid codes, it is required that the reactive current injection should be provided within 150 ms after the beginning or clearance of the fault. During this time window, the consumption of reactive power is forbidden as long as the rms voltage drops below 0.85 p.u..

### 2.3.2. Design of the Virtual Admittance

The virtual admittance of the SPC naturally brings a proportional relationship between the magnitude of the grid voltage drop and the amount of injected reactive current.

The interchanged reactive power between two voltage sources  $e$  and  $v$  through an impedance can be modeled by:

$$Q = \frac{EV}{Z} \cos(\phi - \delta) - \frac{V^2}{Z} \cos(\phi) \quad (14)$$

where  $V$  and  $E$  are the line-to-line rms values of  $v$  and  $e$ ,  $Z$  the impedance,  $\phi$  the impedance angle and  $\delta$  the load angle, which results from the phase angle difference between  $e$  and  $v$ . In the case of the power interchange between a synchronous generator and the grid,  $v$  is the grid voltage,  $e$  is the stator induced voltage, and  $Z$  is the module of the output impedance of the synchronous generator.

Since the output impedance of a synchronous generator is mainly inductive, the impedance angle is close to  $90^\circ$ . Then Equation (14) can be transformed to:

$$Q = \frac{V}{X} (E \cos(\delta) - V) \quad (15)$$

where  $X$  is the reactance of the output impedance.

Equation (15) can be written as Equation (16), considering a small value of  $\delta$ , which represents the operation around the rated condition.

$$Q = \frac{V}{X}(E - V) \quad (16)$$

Therefore, the reactive current injected by the generator will be:

$$I_q = \frac{Q}{V} = \frac{E - V}{X} \quad (17)$$

Therefore, the incremental amount of the injected reactive current will be proportional to the change in the voltage magnitude, namely:

$$\Delta I_q = \frac{-\Delta V}{X} \quad (18)$$

In the case of SPC-based grid-connected power converters, the value of  $X$  can be specified simply by setting the value of the inductance in the virtual admittance block. In order to specify a proper value for such a reactance, the per-unit value of  $X$  is considered and defined as:

$$X_{pu} = \frac{X}{V^2/S_n} = \frac{2\pi fL}{V^2/S_n} \quad (19)$$

Then, Equation (18) can be expressed in per unit as:

$$\Delta I_q^{pu} = \frac{-\sqrt{3}\Delta V_{pu}}{X_{pu}} \quad (20)$$

Based on the knowledge on traditional power systems, a typical value for the output impedance of a synchronous generator,  $X_{pu}$ , can be chosen around 0.3 [29]. Then, according to Equation (20), the resulting proportional gain,  $k_q$ , is calculated to be 5.77. Figure 3 shows the voltage support characteristics when  $X_{pu} = 0.3$  compared with the E.ON and REE grid codes, which set a minimum current that should be provided by a generation unit during the fault. It can be observed in this figure that the resulting voltage support characteristic is above the requirements of both grid codes.

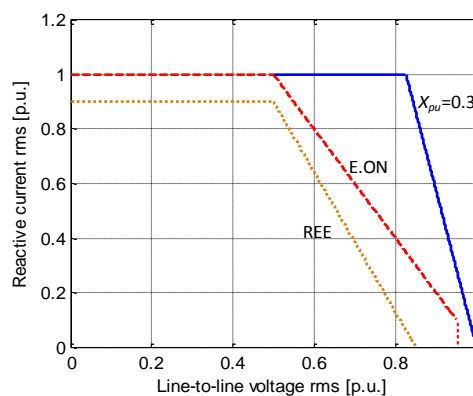


**Figure 3.** The voltage support characteristics when  $X_{pu} = 0.3$  compared with the grid codes' requirements.

Therefore, Figure 3 gives a clue for specifying the values of the positive-sequence admittance, i.e., the first branch in Figure 2. For the purpose of meeting the grid code requirements, the value of  $L_1$  can be calculated based on Equation (19) once  $X_{pu}$  is set. The value for  $R_1$  can be chosen through a dynamic study of the admittance transfer function (1st order low-pass filter) to yield a desired

bandwidth with sufficient damping. Since the proportional gain for negative-sequence current injection can be chosen in a range as indicated by Equation (13),  $L_2$  might be set different from  $L_1$ .

The time response of the virtual admittance block has to be fast enough to achieve an effective voltage regulation. The virtual admittance block contains three selective admittances as shown in Figure 2, for positive-sequence, negative-sequence and transient current regulation, respectively. The transfer function for each branch has the same form and can be generalized as:

$$\frac{\Delta i_{ref}}{\Delta v}(s) = \frac{1}{R_n + sL_n}, \quad n = 1, 2, 3 \quad (21)$$

Then, we can estimate the settling time of the virtual admittance that responds to a variable input. Since in this application the input signals for the admittances,  $\Delta v$ , can be assumed sinusoidal, the time response can be estimated by the response of the magnitude of the two output signals that are generated by giving two sinusoidal input signals in quadrature. The expression is written as:

$$h_V(t) = \sqrt{h_{v\alpha}(t)^2 + h_{v\beta}(t)^2} \quad (22)$$

where  $h_{v\alpha}(t)$  and  $h_{v\beta}(t)$  are the responses to the sinusoidal input signals on  $\alpha$ - and  $\beta$ -axis, respectively, and they can be calculated by the convolution:

$$h_{v\alpha}(t) = v_\alpha \times h_\delta(t) \quad (23a)$$

$$h_{v\beta}(t) = v_\beta \times h_\delta(t) \quad (23b)$$

where  $h_\delta(t)$  is the system impulse response, and  $v_\alpha$  and  $v_\beta$  are:

$$v_\alpha = V \cos(\omega t) \quad (24a)$$

$$v_\beta = V \sin(\omega t) \quad (24b)$$

In practice, the settling time of  $h_V(t)$  has to be calculated with discretized signals (discretized input signal with finite length and discretized transfer function). Providing the calculated response is written as:

$$h_V(k) = \sqrt{h_{v\alpha}(k)^2 + h_{v\beta}(k)^2} \quad (24)$$

then the settling time can be calculated by:

$$t_s = T_s \cdot \max\{ \forall k \quad s.t. \quad \left| \frac{h_V(k)}{h_V(n)} - 1 \right| > \varepsilon_s \} \quad (25)$$

where  $T_s$  is the discretizing sampling time,  $n$  the total number of the points of the discretized signal, and  $\varepsilon_s$  the defined steady-state band.

Specifying the values for  $R_{pu}$  and  $X_{pu}$  to be 0.1 p.u. and 0.3 p.u., respectively, the settling time for the admittance expression,  $\frac{1}{R+jX}$ , is 21.6 ms, which is calculated according to the aforementioned method, with  $\varepsilon_s = 0.1$ . This settling time can indicate the response of the transient admittance branch, namely, the second branch of the virtual admittance block in Figure 2. For the other two branches that deal with positive- and negative-sequence voltages, the time response is also dependent on the filtering stage of the virtual admittance block (as shown in Figure 2). The time response of the sequence filtering stages can be determined from Equations (10) and (11).

Figure 4a shows the response of the sequence filter for the negative-sequence rms component for different values of the bandwidth parameter  $k_{bw}$ .

According to Equation (11), the response for the positive-sequence component will have the same characteristics in time. Therefore, by tuning the  $k_{bw}$  in Equation (11), the speed for separating the positive- and negative-sequence components of the grid voltage can be easily adjusted.

Figure 4b shows how the dynamics of the positive- and negative-sequence current injection during asymmetrical faults is mainly determined by the sequence filtering stage, since the admittance time response is very fast and does not add almost any delay.

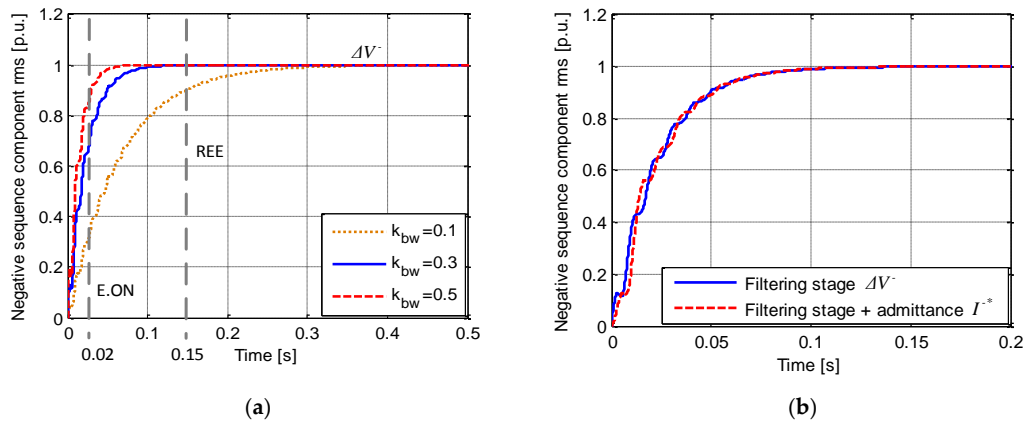


**Figure 4.** The time response of: (a) the sequence filtering stage of the virtual admittance block under different values of  $k_{bw}$ ; and (b) the virtual admittance block when  $k_{bw} = 0.3$ .

### 3. Simulation Results

Simulation tests based on a digital implementation of the proposed controller are presented firstly in this section. A 100 kW two-level three-phase converter connected to a 400 V/50 Hz grid through a grid link filter is modeled for simulation, as shown in Figure 5. The key parameters for the test setup and controller are listed in Table 1.

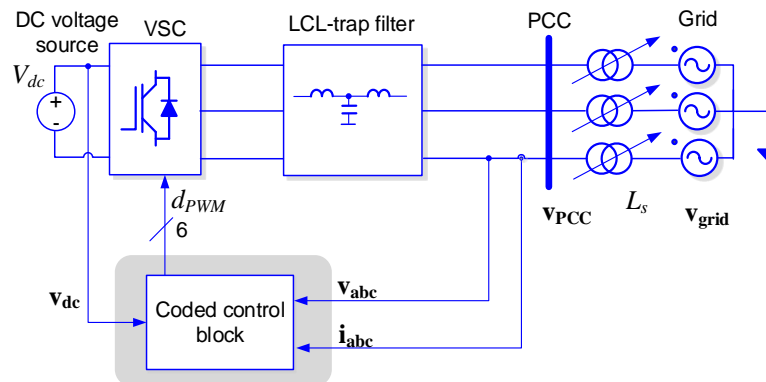


**Figure 5.** The 100 kW grid-connected power converter simulation test system.

**Table 1.** Key parameters of the 100 kW SPC-based power converter.

Description	Symbol	Value
DC voltage	$V_{dc}$	750 [V]
Sag generator equivalent inductance	$L_s$	800 [ $\mu$ H]
Switching frequency	$f_{sw}$	3150 [Hz]
Virtual resistance	$R_{pu}$	0.1 [p.u.]
Virtual reactance	$X_{pu}$	0.3 [p.u.]
Sequence filtering stage bandwidth	$k_{bw}$	0.3
SPC's virtual inertia constant	$H$	5 [s]
SPC's virtual damping factor	$\zeta$	0.7

The event considered in this simulation test is a 0.43 p.u. of voltage sag in one of the phases of the ac source, and it lasts for 200 ms. According to the aforementioned grid codes, the power converter should remain connected to the grid under such unbalanced voltage drop and the voltage support should be also triggered.

A generalized expression for the current reference generated by the virtual admittance block can be written as:

$$\mathbf{i}^* = \frac{1}{R + Ls} (A_{pos}\Delta\mathbf{v}^+ + A_{neg}\Delta\mathbf{v}^- + A_{trans}\Delta\mathbf{v}_{trans}) \quad (26)$$

where  $L$  and  $R$  are the unified inductance and resistance that can be calculated based on the specified  $X_{pu}$  and  $R_{pu}$ .

To set different values for each sequence admittance in the virtual admittance block, the unified value of resistance and inductance can be modified by different coefficients, as shown in Equation (27). In this way, the admittance value for each branch can be simply defined by specifying value for the coefficients  $A_{pos}$ ,  $A_{neg}$  and  $A_{trans}$ . Therefore, the inductance and resistance in each branch have the values shown in Table 2.

**Table 2.** The inductance and resistance in each branch.

Description	Symbol	Value
Positive sequence resistance	$R_1$	$R/A_{pos}$
Positive sequence inductance	$L_1$	$L/A_{pos}$
Negative sequence resistance	$R_2$	$R/A_{neg}$
Negative sequence inductance	$L_2$	$L/A_{neg}$
Transient resistance	$R_3$	$R/A_{trans}$
Transient inductance	$L_3$	$L/A_{trans}$

Once  $X_{pu}$  and  $R_{pu}$  are set to meet requirements in reactive current injection during the faults,  $A_{pos}$  can be set to 1 by convenience.

In the experiments, two different sets of values for the virtual admittances are specified. In the first case, the value for  $A_{neg}$  was set to 10, which is a significantly greater value than the ones for  $A_{pos}$  and  $A_{trans}$  (which were both set to 1 by convenience), to clearly boost the negative-sequence current injection in the case of unbalanced faults. In contrast, the value for  $A_{neg}$  was set to 0.1 in a second case to limit the injection of negative-sequence current injection during unbalanced faults. These very different values for  $A_{neg}$ , namely 10 and 0.1, were chosen in this study case to clearly evidence the effect of the negative-sequence admittance value during unbalanced faults. However, in real applications,  $A_{neg}$  should be determined according to the TSO requirements on the ratio between  $V^-$  and  $I^-$ .

Working with the first set of values, i.e. with  $A_{neg} = 10 A_{pos}$ , it can be clearly appreciated in Figure 6 how the power converter provides a significant support to recover the voltage at the PCC,  $\mathbf{v}_{PCC}$ , regarding both magnitude and symmetry recovery. By using such a large value for the negative-sequence admittance, the unbalanced voltage at the PCC is almost compensated as Figure 6b shows, compared to the grid voltage  $\mathbf{v}_{grid}$ , as Figure 6a shows. The highly unbalanced current injected to the grid, shown in Figure 6c, denotes its large negative-sequence component.

Considering the second set of values, a small value for the negative-sequence admittance is used,  $A_{neg} = 0.1 A_{pos}$ , hence the converter injects a very limited amount of negative-sequence current during the unbalanced fault, which is denoted by the relatively balanced current waveforms shown in Figure 7c. As a result, the PCC voltage unbalance is almost not compensated during the unbalanced grid fault as Figure 7b shows. Setting a low value for  $A_{neg}$  can be needed in practice considering current limitations of the power converter. Hence, small size power converters will be mainly responsible for positive-sequence current injection.

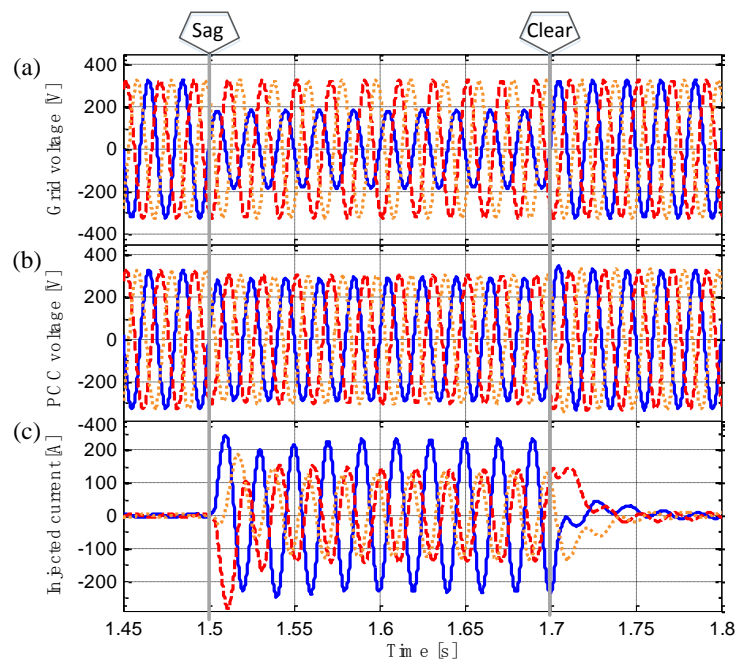


**Figure 6.** Response of the SPC-based power converter under an asymmetrical grid fault when  $A_{pos} = 1$ ,  $A_{neg} = 10 A_{pos}$ : (a) grid voltage; (b) point of common coupling (PCC) voltage; and (c) current injected by the converter.

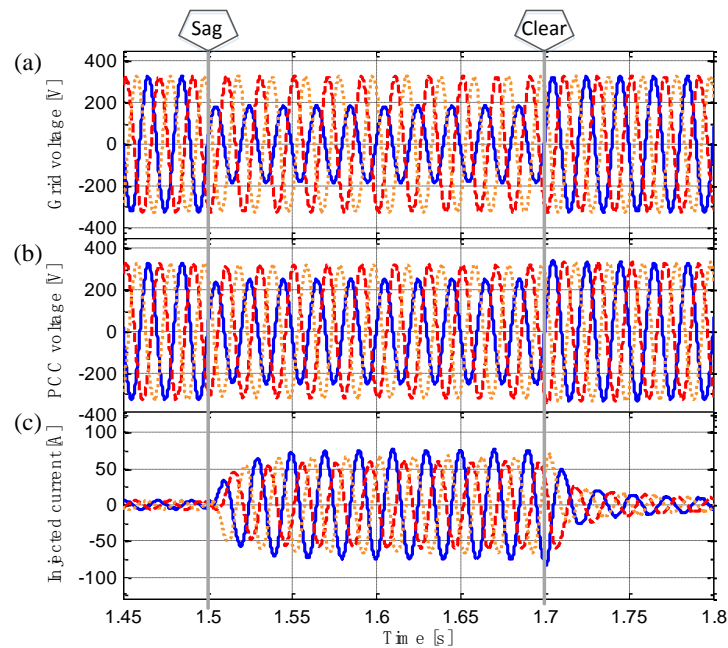


**Figure 7.** Response of the SPC-based power converter under an asymmetrical grid fault when  $A_{pos} = 1$ ,  $A_{neg} = 0.1 A_{pos}$ : (a) grid voltage; (b) PCC voltage; and (c) current injected by the converter.

The rms value for the positive- and negative-sequence components of the voltage at the PCC and the injected current, calculated by  $V_{rms}^+ = \sqrt{\frac{1}{3}(v_{\alpha}^{+2} + v_{\beta}^{+2})}$  and  $V_{rms}^- = \sqrt{\frac{1}{3}(v_{\alpha}^{-2} + v_{\beta}^{-2})}$ , are shown in Figure 8.

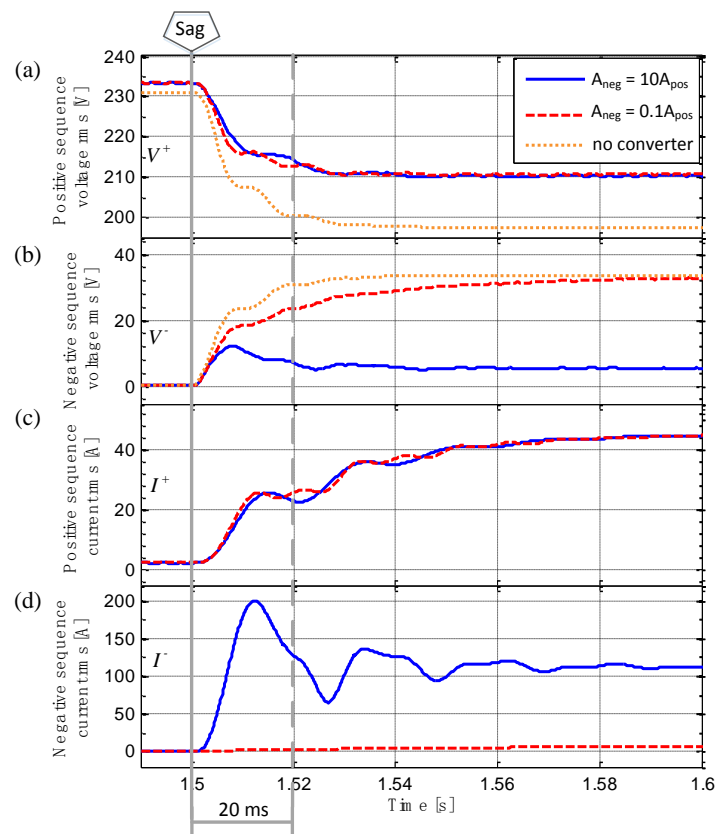


**Figure 8.** Comparison of the unbalanced voltage support effect of the SPC-based power converter under different negative-sequence virtual admittances: (a) positive sequence PCC voltage rms; (b) negative sequence PCC voltage rms; (c) positive sequence current rms; and (d) negative sequence current rms.

Figure 8a shows that the positive-sequence voltage is properly supported by the SPC-based power converter with virtual admittance. The drop of the positive-sequence voltage component at the PCC is 8.5% when the power converter is activated, in comparison with 14.1% when the power converter is blocked. Figure 8b demonstrates a significant compensation of the unbalanced effect. When  $A_{neg} = 10$ , the per-unit rms voltage of the negative-sequence at the PCC during the fault is only 2.35%, a value much smaller than 14.6%, which is the per-unit rms voltage of the negative-sequence component of the voltage at the main grid. Figure 8d shows that the rms value of the negative-sequence current injected during the unbalanced fault can be simply adjusted by changing the values for the negative-sequence admittance, i.e.,  $A_{neg}$ . Figure 8 also shows that the reaction of the converter in presence of the unbalanced fault is less than 20 ms and gets settled within 100 ms, which meets the grid codes requirements.

Figure 9 shows the effect of the transient admittance branch in the proposed virtual admittance block.  $A_{trans}$  is set to 0 and 1 in two different study cases, while  $A_{pos}$  is set to 1 and  $A_{neg}$  is set to 10 in both cases. As seen in Figure 9, the transient admittance contributes to a faster response when the unbalanced fault takes place. The injected current responds faster when the transient admittance is enabled, and both positive- and negative-sequence components of the PCC voltage present a smoother change than in the case of disabling the transient impedance. The coherence of the steady-state profiles in each scope of Figure 9 shows that the static performance is not affected by the transient admittance.

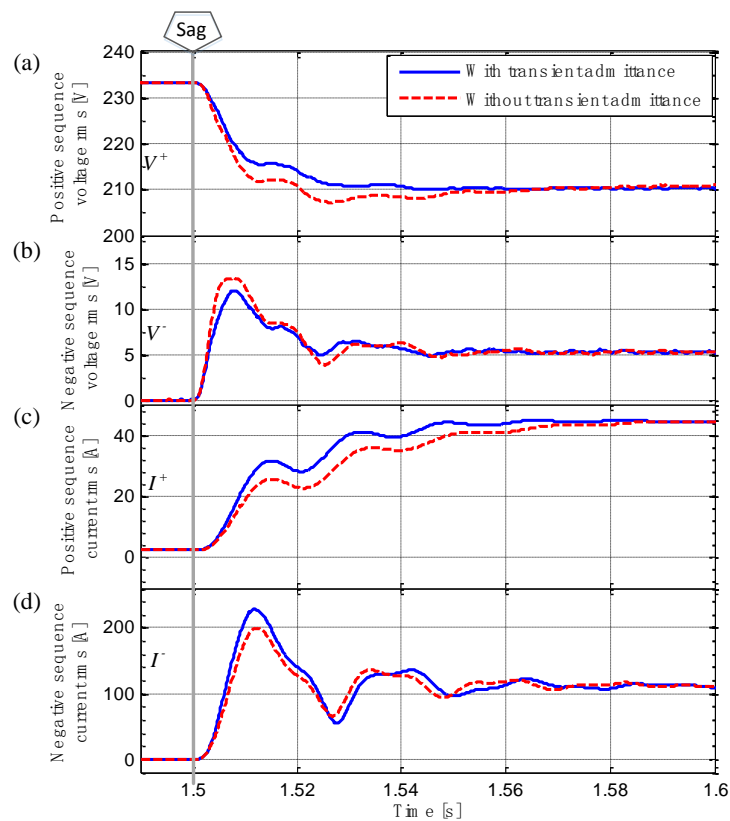


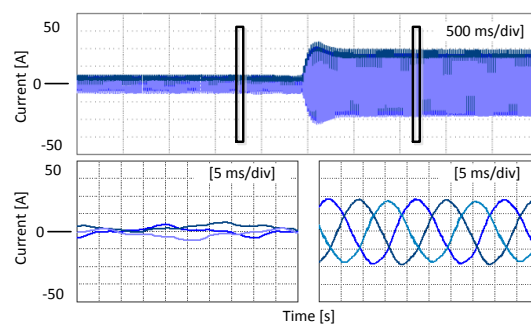
**Figure 9.** Effect of the transient admittance branch under an asymmetrical grid fault: (a) positive sequence PCC voltage rms; (b) negative sequence PCC voltage rms; (c) positive sequence current rms; and (d) negative sequence current rms.

#### 4. Experimental Results

As a first test scenario, a 10 kW grid-connected power converter is used to check whether the SPC controlled power converter can start-up and injects the power correctly with good dynamics.

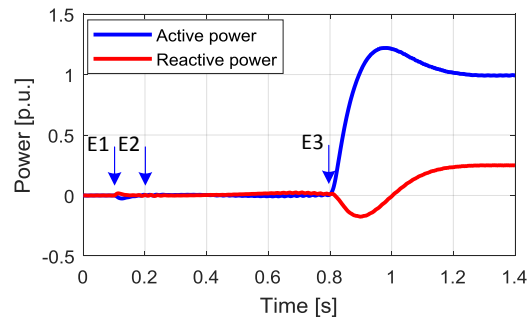
The converter is programmed to have small virtual admittances in all the three branches of the virtual admittance block initially, being  $A_{pos} = A_{neg} = A_{trans} = 0.01$ , in order to minimize the transient at the instant of grid connection. Then, the virtual admittance parameters gradually increase to 1 after the switching is enabled. Then, the active and reactive power references jump from 0 to 10 kW and 2.5 kVar afterwards.

Figure 10 shows the current waveforms during the whole process. It is seen that no transient of current is found at the instant when the converter's switching is enabled, and no oscillations of current are found during the admittance parameters changing and the active power step-up.



**Figure 10.** Waveforms of the current injected by the power converter during start-up and power step-up.

Figure 11 shows the active and reactive power injected by the power converter during the whole process. At  $t = 0.1$  s, the power converter's switching is enabled (E1). At  $t = 0.2$  s, the admittance parameters start increasing from the value 0.01, and reach the value 1 at  $t = 0.7$  s. At  $t = 0.8$  s, the active and reactive power references jump from 0 to 10 kW and 2.5 kVar. It is observed how the power injected by the converter is correctly controlled free from oscillations or significant deviations during the whole process.



**Figure 11.** Active and reactive power injected by the power converter during the start-up and power step-up.

The above experimental results have demonstrated the correct implementation of the overall SPC control scheme. Then, the following tests are oriented to show the performance of the proposed virtual admittance block under asymmetrical grid fault.

Figure 12 shows the experimental setup for asymmetrical grid fault tests, where two 100 kW two-level three-phase power converters with the same specifications are connected in parallel and to the utility grid through a sag generator. The setup is pictured in Figure 13. A dc power source supplies both converters. The parameters for the SPC-based power converters are the same as the ones used in simulation, shown in Table 1. The event considered in the experiments is the same with the simulation tests, namely, a voltage sag of 0.43 p.u. in one of the phases of the ac grid.

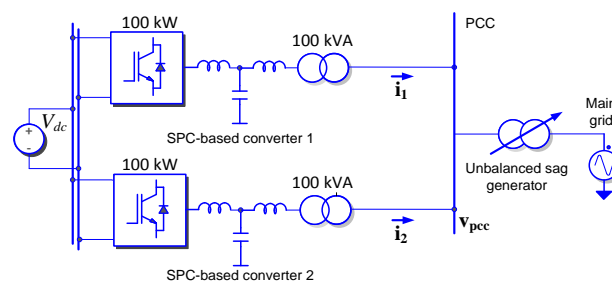


**Figure 12.** Experimental setup for unbalanced voltage sag tests.

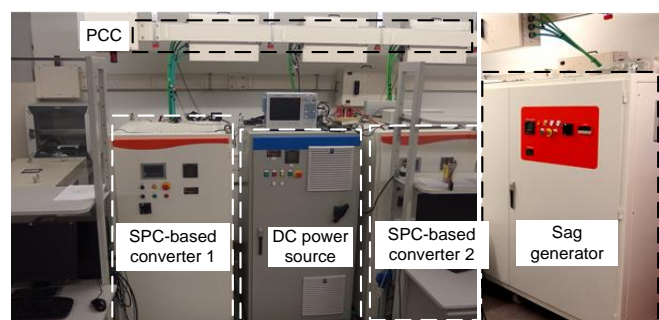


**Figure 13.** Laboratory view of the asymmetrical grid fault experimental setup.

In a first experiment, only one of the two converters is connected, and  $A_{pos}$ ,  $A_{neg}$ , and  $A_{trans}$  are set to 1, 10 and 1, respectively. The voltage and current waveforms at the PCC during normal working and under fault conditions are shown in Figure 14. In this experimental test, the voltage sag is started and ended manually, which lasts for 8 s.

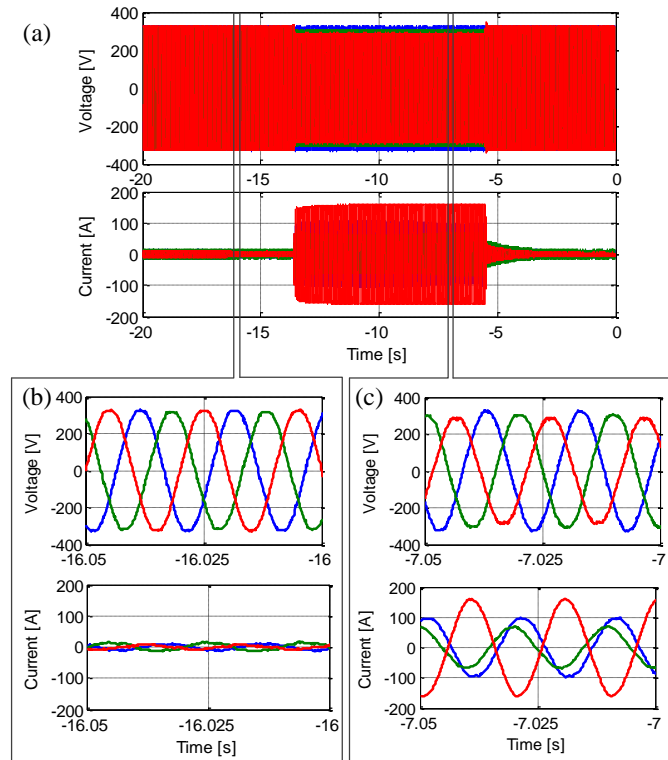


**Figure 14.** Single SPC-based converter working. The PCC voltage and current injection when  $A_{pos} = 1$  and  $A_{neg} = 10 A_{pos}$ : (a) the whole experimental process; (b) prior to the fault; and (c) during the fault.

Figure 14a shows the envelope of the PCC voltage and converter injected current before, during and after the fault. A zoom-in of the pre-fault voltage and current waveforms are shown in Figure 14b, while the zoom-in voltage and current waveforms during the fault are shown in Figure 14c. These plots evidence how the PCC voltage is well supported during the unbalanced fault. There are only minor visible differences in the voltage waveforms magnitude before and during the fault. Therefore, it is demonstrated how the injected negative-sequence current results in relatively balanced voltage waveforms at the PCC.

The recorded data from the oscilloscope are plotted in Figure 15 to check the power converter dynamics and a quantitative evaluation of the injected positive- and negative-sequence currents. The positive- and negative-sequence components of the PCC voltage are also calculated.

From the profiles of the rms current of the positive- and negative-sequence components, as Figure 15d shows, the fast reaction of the power converter to support the unbalanced grid voltage can be appreciated. The positive- and negative-sequence current raised to 68% and 62% of the steady-state value, respectively, just 20 ms after of the fault start.

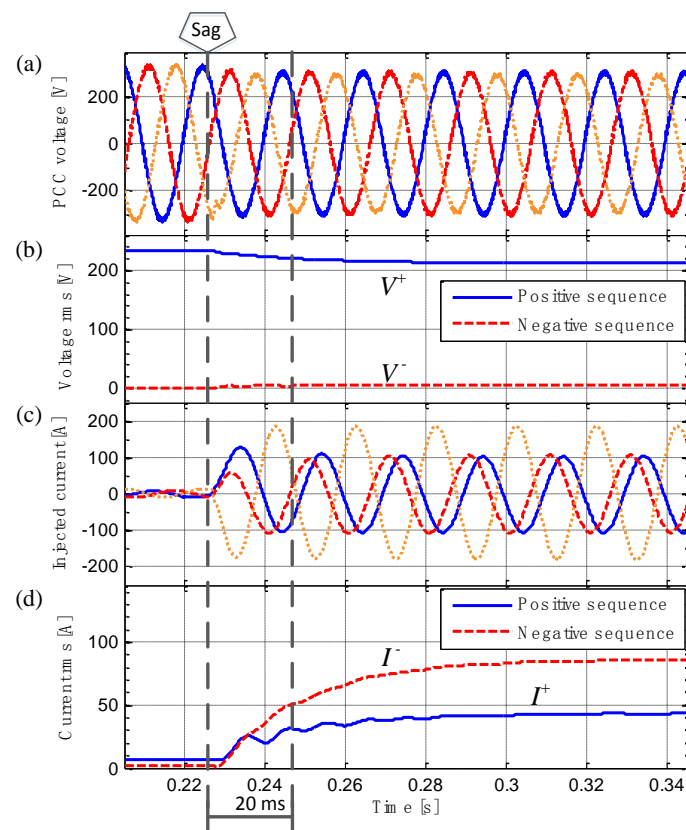
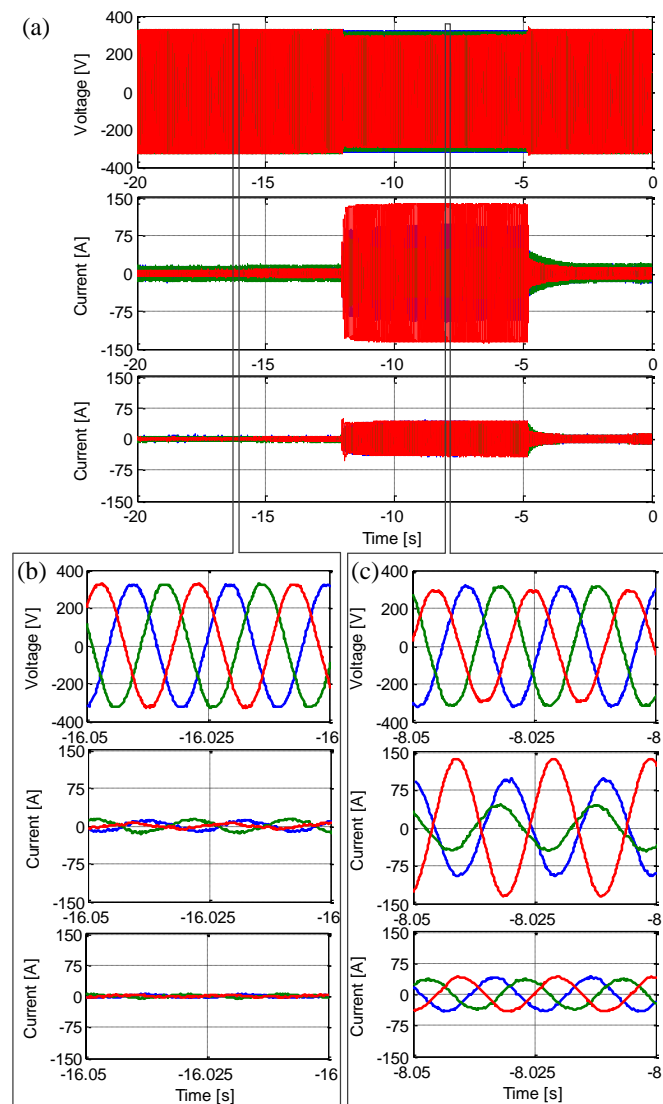


**Figure 15.** Single SPC-based power converter working. Transient response after the start of an unbalanced sag: (a) voltage at the PCC; (b) positive- and negative-sequence voltage rms; (c) current injected by the converter; and (d) positive- and negative-sequence current rms.

In a second experimental test, both converters are connected to the grid in order to test current sharing performance in front of common disturbances. The positive- and transient-admittance values were set the same for both converters, while different values for  $A_{neg}$  were set for the two power converters, i.e.,  $A_{neg} = 10 A_{pos}$ , and  $A_{neg} = 0.1 A_{pos}$ , respectively.

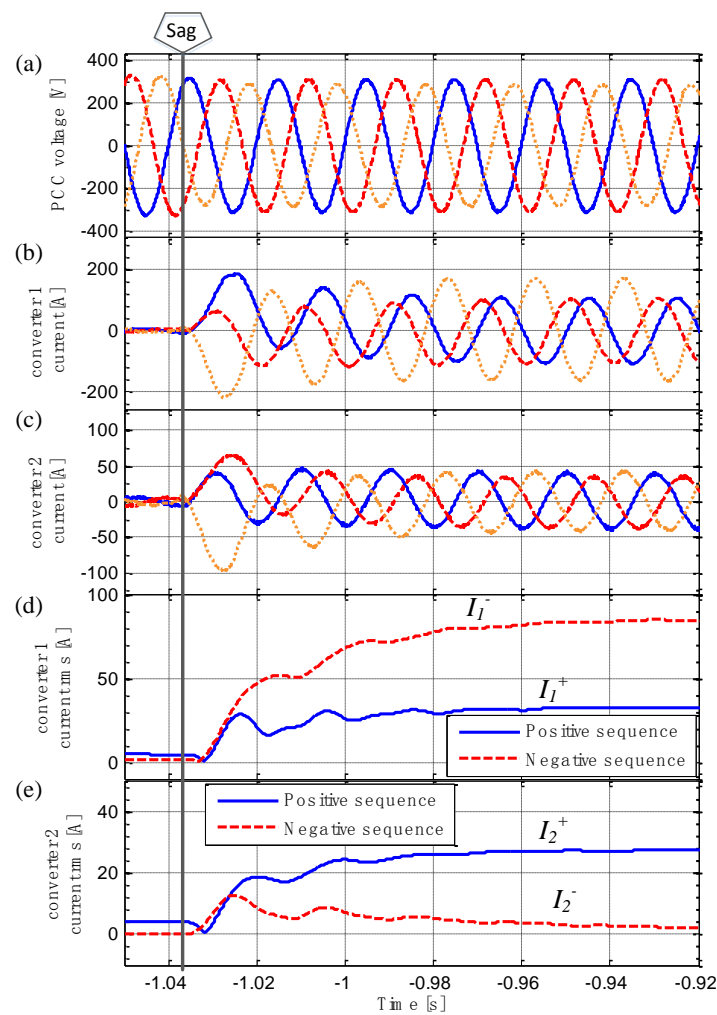
Figure 16 shows the difference in the current injection of the two power converters when different values for  $A_{neg}$  are set in both converters. For converter 1, with  $A_{neg} = 10$ , the injected current during the fault has unbalanced waveforms as Figure 16c shows, since it contains a large amount of negative-sequence component. For converter 2, with  $A_{neg} = 0.1$ , the injected current during the fault is relatively balanced, due to the small rate of negative-sequence current injection. Thanks to the combined support provided by both converters, the voltage at the PCC does not experience a significant change in magnitude during the grid fault, which can be seen by comparing Figure 16b,c.

Figure 17 compares the rms value of the current injected by both converters. Since both of them have the same value for  $A_{pos}$ , the rms value of the positive-sequence current component is at the same level in both converters. However, the negative-sequence rms current profiles for both converters exhibit a clear difference in magnitude. It practically demonstrates that negative-sequence current sharing among paralleled converter can be easily adjusted by just setting proper values for  $A_{neg}$  in each of them.



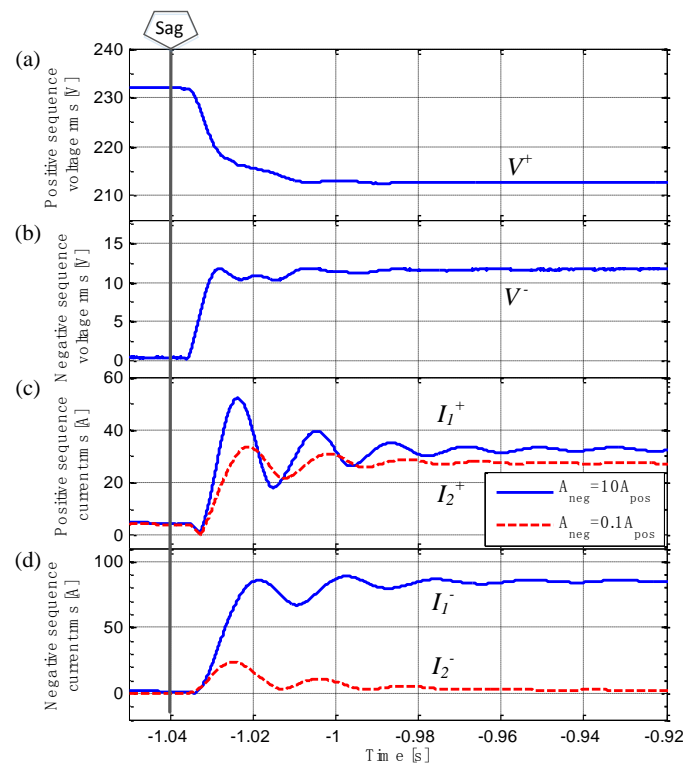
**Figure 16.** Two SPC-based converters working with different negative-sequence virtual admittances. The PCC voltage and current injection: (a) the whole experimental process; (b) prior to the fault; and (c) during the fault.

Figure 18 shows the rms profile of the positive- and negative-sequence components of the voltage at the PCC and the currents injected by two power converters with different negative-sequence virtual admittances. The positive-sequence voltage drop at the PCC, as Figure 18a shows, is equal to 8.3% of its rated value, which is much smaller than the positive-sequence grid voltage drop, which is equal to 13.8%. Since the two converters have the same value for  $A_{pos}$ , the steady-state value of  $I_1^+$  and  $I_2^+$  are close each other as Figure 18c shows. However, converter 1 injects much more amount of negative-sequence current than converter 2 as Figure 18d shows, due to the high value set for  $A_{neg}$  in the former. The negative-sequence voltage component at the PCC increases by 5.2% during the fault. It is worth noting that even though the negative-sequence voltage component at the PCC, as Figure 18b shows, is 5.2%, which is smaller than the one in grid voltage (14.6%) during the unbalanced fault, it is greater than the one in the former experiment, when converter 2 was not connected (1.9%). Therefore, the relative influence of converter 1 on the PCC voltage is reduced due to the participation of converter 2.



**Figure 17.** Two SPC-based power converters working with different negative-sequence virtual admittances. The transient responses after the start of an unbalanced sag: (a) voltage at the PCC; (b) current injected by the converter 1; (c) current injected by the converter 2; (d) rms of the positive- and negative-sequence current injected by the converter 1; and (e) rms of the positive- and negative-sequence current injected by the converter 2.

Based on the steady-state rms value for the positive- and negative-sequence voltage and current components, the actual gain of the negative-sequence current injection ( $\Delta I^- / \Delta V^-$ ) obtained from experimental results can be calculated. The actual gains for the two converters are visualized in Figure 19 and compared with requirements in the Verband der Elektrotechnik (VDE) grid codes (considering a 5% dead-band for each one). As can be observed in Figure 19, the characteristics of the two converters are within the range of the grid codes requirements (the shadow area).



**Figure 18.** Two SPC-based converters working with different negative-sequence virtual admittances. Comparison of the negative-sequence current injection of the two converters during an unbalanced sag: (a) positive sequence PCC voltage rms; (b) negative sequence PCC voltage rms; (c) positive sequence current rms; and (d) negative sequence current rms.

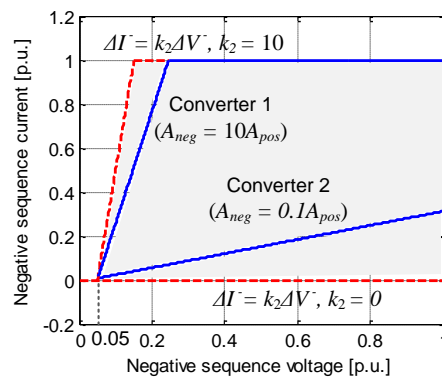


**Figure 19.** Two SPC-based power converters working with different negative sequence virtual admittances. The  $V^- - I^-$  slope of the two converters compared with the VDE grid codes.

### 5. Conclusions

This paper presents a virtual admittance controller aimed to provide voltage support under asymmetrical grid faults. By using independent and selective admittances for positive- and negative-sequence current injection, the unbalanced voltage can be significantly conditioned during asymmetrical faults. This controller is based on the general control framework of the SPC, which is able to control a grid-connected power converter with emulated and improved synchronous generator characteristics. Simulation and experimental results showed the significant effect of the proposed controller for unbalanced grid voltage support. A desired droop ratio for positive- and negative-sequence current injection to meet the grid codes can be easily achieved by adjusting

the values of the positive- and negative-sequence admittance, respectively. The time response of the converter in presence of the asymmetrical faults can also be tuned for fast voltage support. Further, the transient admittance makes the converter have a faster response when the fault takes place.

**Acknowledgments:** This work has been partially supported by the Spanish Ministry of Economy and Competitiveness under the Project ENE2014-60228-R and ENE2013-48428-C2-2-R. Any opinions, findings and conclusions or recommendations expressed in this material are those of the authors and do not necessarily reflect those of the host institutions or funders.

**Author Contributions:** Pedro Rodriguez proposed the control strategy, provided supervision and revised the paper. Joan Rocabert conducted the analysis, validated the control strategy in experiments and revised the paper. Weiyi Zhang contributed to the analysis, validated the control strategy in simulations and conducted the writing of the paper. J. Ignacio Candela contributed to the analysis, simulations and experiments.

**Conflicts of Interest:** The authors declare no conflict of interest.

## References

1. Blaabjerg, F.; Teodorescu, R.; Liserre, M.; Timbus, A.V. Overview of control and grid synchronization for distributed power generation systems. *IEEE Trans. Ind. Electron.* **2006**, *53*, 1398–1409. [[CrossRef](#)]
2. Holmes, D.G.; Lipo, T.A.; McGrath, B.P.; Kong, W.Y. Optimized design of stationary frame three phase AC Current regulators. *IEEE Trans. Power Electron.* **2009**, *24*, 2417–2426. [[CrossRef](#)]
3. Wen, B.; Dong, D.; Boroyevich, D.; Burgos, R.; Mattavelli, P.; Shen, Z. Impedance-based analysis of grid-synchronization stability for three-phase paralleled converters. *IEEE Trans. Power Electron.* **2015**, *31*, 26–38. [[CrossRef](#)]
4. Buso, S.; Mattavelli, P. *Digital Control in Power Electronics*; Morgan & Claypool: San Rafael, CA, USA, 2006.
5. Bevrani, H.; Ghosh, A.; Ledwich, G. Renewable energy sources and frequency regulation: Survey and new perspectives. *IET Renew. Power Gener.* **2010**, *4*, 438. [[CrossRef](#)]
6. Driesen, J.; Visscher, K. Virtual synchronous generators. In Proceedings of the IEEE PES General Meeting, Pittsburgh, PA, USA, 20–24 July 2008; pp. 1–3.
7. Zhang, L.; Harnefors, L.; Nee, H.P. Power-synchronization control of grid-connected voltage-source converters. *IEEE Trans. Power Syst.* **2010**, *25*, 809–820. [[CrossRef](#)]
8. Zhang, L.; Harnefors, L.; Nee, H.P. Interconnection of two very weak AC systems by VSC-HVDC links using power-synchronization control. *IEEE Trans. Power Syst.* **2011**, *26*, 344–355. [[CrossRef](#)]
9. Network Code for Requirements for Grid Connection Applicable to all Generators. Available online: <http://www.acer.europa.eu/Media/News/Documents/120626%20-%20NC%20RfG%20-%20Frequently%20Asked%20Questions%20%282%29.pdf> (accessed on 7 July 2017).
10. Alatrash, H.; Mensah, A.; Mark, E.; Haddad, G.; Enslin, J. Generator emulation controls for photovoltaic inverters. *IEEE Trans. Smart Grid* **2012**, *3*, 996–1011. [[CrossRef](#)]
11. Hirase, Y.; Abe, K.; Sugimoto, K.; Shindo, Y. A grid-connected inverter with virtual synchronous generator model of algebraic type. *Electr. Eng. Jpn.* **2013**, *184*, 10–21. [[CrossRef](#)]
12. Alipoor, J.; Miura, Y.; Ise, T. Power system stabilization using Virtual synchronous generator with alternating moment of inertia. *IEEE J. Emerg. Sel. Top. Power Electron.* **2015**, *03*, 451–458. [[CrossRef](#)]
13. Mahmood, H.; Michaelson, D.; Jiang, J. Accurate reactive power sharing in an islanded microgrid using adaptive virtual impedances. *IEEE Trans. Power Electron.* **2014**, *30*, 1605–1617. [[CrossRef](#)]
14. Paquette, A.D.; Divan, D.M. Virtual impedance current limiting for inverters in microgrids with synchronous generators. *IEEE Trans. Ind. Appl.* **2015**, *51*, 1630–1638. [[CrossRef](#)]
15. He, J.; Li, Y.W.; Munir, M.S. A flexible harmonic control approach through voltage-controlled DG-grid interfacing converters. *IEEE Trans. Ind. Electron.* **2012**, *59*, 444–455. [[CrossRef](#)]
16. Wang, X.; Blaabjerg, F.; Chen, Z. Synthesis of variable harmonic impedance in inverter-interfaced distributed generation unit for harmonic damping throughout a distribution network. *IEEE Trans. Ind. Appl.* **2012**, *48*, 1407–1417. [[CrossRef](#)]
17. Zhang, X.; Zhong, Q.; Ming, W. Stabilization of a cascaded DC converter system via adding a virtual adaptive parallel impedance to the input of the load converter. *IEEE Trans. Power Electron.* **2016**, *31*, 1826–1832. [[CrossRef](#)]

18. Bollen, M.H.J. Characterisation of voltage sags experienced by three-phase adjustable-speed drives. *IEEE Trans. Power Deliv.* **1997**, *12*, 1666–1671. [[CrossRef](#)]
19. Engelhardt, S.; Kretschmann, J.; Fortmann, J.; Shewarega, F.; Erlich, I.; Feltes, C. Negative sequence control of DFG based wind turbines. In Proceedings of the IEEE PES General Meeting, Detroit, MI, USA, 24–29 July 2011; pp. 1–8.
20. Wang, W.; Ma, X. Transient analysis of low-voltage ride-through in three-phase grid-connected converter with LCL filter using the nonlinear modal series method. *Electr. Power Syst. Res.* **2013**, *105*, 39–50. [[CrossRef](#)]
21. Tang, C.; Chen, Y.; Chen, Y. PV power system with multi-mode operation and low-voltage ride-through capability. *IEEE Trans. Ind. Electron.* **2015**, *62*, 7524–7533. [[CrossRef](#)]
22. Wijnhoven, T.; Deconinck, G. Flexible fault current contribution with inverter interfaced distributed generation. In Proceedings of the IEEE PES General Meeting, Vancouver, BC, Canada, 21–25 July 2013.
23. Teodorescu, R.; Liserre, M.; Rodriguez, P. *Grid Converters for Photovoltaic and Wind Power Systems*; John Wiley & Sons: Hoboken, NJ, USA, 2011.
24. Gabe, I.J.; Fábio, F.; Palha, K.; Pinheiro, H. Grid connected voltage source inverter control during voltage dips. In Proceedings of the IECON'09. 35th Annual Conference of IEEE Industrial Electronics, Porto, Portugal, 3–5 November 2009.
25. Rodriguez, P.; Luna, A.; Ciobotaru, M.; Teodorescu, R.; Blaabjerg, F. Advanced grid synchronization system for power converters under unbalanced and distorted operating conditions. In Proceedings of the IECON 2006-32nd Annual Conference on IEEE Industrial Electronics, Paris, France, 6–10 November 2006; pp. 5173–5178.
26. *Requirements for Offshore Grid Connections in the E.ON Netz Network*; E.ON Netz GmbH: Bayreuth, Germany, 2008.
27. Fuentes, J.A.; Cañas, M.; Molina, A.; Gómez, E.; Jiménez, F. International Review of Grid Connection Requirements Related With Voltage Dips for Wind Farms. Available online: <http://icrepq.com/icrepq07/330-fuentes.pdf> (accessed on 7 July 2017).
28. Wijnhoven, T.; Neumann, T.; Deconinck, G.; Erlich, I. Control aspects of the dynamic negative sequence current injection of type 4 wind turbines. In Proceedings of the IEEE PES General Meeting, National Harbor, MD, USA, 27–31 July 2014.
29. Anderson, P.M.; Fouad, A.A. *Power System Control and Stability*; John Wiley & Sons: Hoboken, NJ, USA, 2002.



© 2017 by the authors. Licensee MDPI, Basel, Switzerland. This article is an open access article distributed under the terms and conditions of the Creative Commons Attribution (CC BY) license (<http://creativecommons.org/licenses/by/4.0/>).